Tracking bubble evolution inside a silicic dike

DOI:
10.1016/j.lithos.2016.08.012

Citation for published version (APA):
Álvarez-Valero, A. M., Okumura, S., Arzilli, F., Borrajo, J., Recio, C., Ban, M., Gonzalo, J. C., Benítez, J. M., Douglas, M., Sasaki, O., Franco, P., Gómez-Barreiro, J., & Carnicero, A. (2016). Tracking bubble evolution inside a silicic dike. *Lithos*, *262*, 668-676. https://doi.org/10.1016/j.lithos.2016.08.012

Published in:
Lithos

Elsevier Editorial System(tm) for Lithos
Manuscript Draft

Manuscript Number: LITHOS5319R2

Title: Tracking bubble evolution inside a silicic dike

Article Type: Regular Article

Keywords: Volcanic bubbles; Dacite; X-ray micro-tomography; Crustal xenoliths; Conduit depths; Stable Isotopes

Corresponding Author: Dr. Antonio M. Álvarez-Valero,

Corresponding Author's Institution: Universidad de Salamanca

First Author: Antonio M. Álvarez-Valero

Order of Authors: Antonio M. Álvarez-Valero; Satoshi Okumura; Fabio Arzilli; Javier Borrajo; Clemente Recio; Masao Ban; Juan Carlos Gonzalo; Jose Benítez; Madison Douglas; Osamu Sasaki; Piedad Franco; Juan Gómez-Barreiro; Asunción Carnicero

Abstract: Pressure estimates from rapidly erupted crustal xenoliths constrain the depth of intrusion of the silicic lavas hosting them. This represents an opportunity for tracking magmatic bubble's evolution and quantifying the variation in bubble volume during rapid magma ascent through a volcanic dike just prior to eruption. The petrology, stable-isotope geochemistry and X-ray micro-tomography of dacites containing crustal xenoliths, erupted from a Neogene volcano in SE Spain, showed an increase in porosity from ~1.7 to 6.4 % from ~19 to 13 km depth, at nearly constant groundmass and crystal volumes. This result provides additional constraints for experimental and numerical simulations of subvolcanic magma-crust degassing processes in silicic systems, and may allow the characterization of volcanic eruptive styles based on volatile content.

***Highlights (for review)**

Direct observation of bubbles in a natural-silicic volcano-laboratory

Combination of petrology, geochemistry and micro-computed-tomography

Bubbles evolution in the magma dike from 19 to 13 km depth

Implications for the volatiles influence in the eruptive processes at higher depths than the usually considered for the volcanic vent

Tracking bubble evolution inside a silicic dike

Antonio M. Álvarez-Valero[1*], Satoshi Okumura[2], Fabio Arzilli[3], Javier Borrajo[4], Clemente Recio[1], Masao Ban[5], Juan C. Gonzalo[1], José M. Benítez[1], Madison Douglas[6], Osamu Sasaki[7], Piedad Franco[1], Juan Gómez-Barreiro[1], Asunción Carnicero[1]

[1] Department of Geology, Faculty of Sciences, University of Salamanca, Spain

([*]corresponding author: aav@usal.es)

[2] Division of Earth and Planetary Materials Science, Department of Earth Science, Graduate School of Science, Tohoku University, Sendai, Miyagi, Japan

[3] School of Earth, Atmospheric and Environmental Sciences, University of Manchester, UK

[4] Department of Physics, Engineering and Medical Radiology, University of Salamanca, Spain

[5] Department of Earth and Environmental Sciences, Yamagata University, Japan

[6] Department of Earth, Atmospheric and Planetary Sciences, MIT, Cambridge, MA, USA

[7] Division of GeoEnvironmental Science, Department of Earth Science, Graduate School of Science, Tohoku University, Sendai, Miyagi, Japan

ABSTRACT

Pressure estimates from rapidly erupted crustal xenoliths constrain the depth of intrusion of the silicic lavas hosting them. This represents an opportunity for tracking magmatic bubble's evolution and quantifying the variation in bubble volume during rapid magma ascent through a volcanic dike just prior to eruption. The petrology, stable-isotope geochemistry and X-ray micro-tomography of dacites containing crustal xenoliths, erupted from a Neogene volcano in SE Spain, showed an increase in porosity from ~1.7 to 6.4 % from ~19 to 13 km depth, at nearly constant groundmass and crystal volumes. This result provides additional constraints for experimental and numerical simulations of subvolcanic magma-crust degassing processes in silicic systems, and may allow the characterization of volcanic eruptive styles based on volatile content.

Keywords: Volcanic bubbles; Dacite; X-ray micro-tomography; Crustal xenoliths; Conduit depths; Stable Isotopes

1. Introduction

Processes occurring in the conduit between a magma chamber and the surface may trigger an eruption or alter the characteristics of one already in progress (e.g. Costa et al., 2007; 2009). In this regard, gases and fluids play a crucial. The understanding of how gases behave and influence the eruptive style of volcanoes is mainly based on observations of volcanic products, numerical models, and laboratory experiments (e.g., Eichelberger et al., 1986; Jaupart and Allègre, 1991; Woods and Koyaguchi, 1994; Klug and Cashman, 1996; Okumura et al., 2009; Fiege et al., 2014; Fiege and Cichy, 2015). However, the evolution of magmatic gases and fluids immediately prior to eruption is difficult to understand due to the complexity of observing magmatic activity below the surface. While shallower volcanic vents have been investigated through the analysis and experimental reproduction of pyroclastic products (e.g., Valentine, 2012), interactions between the crust and magma at depth (from c. 4 to 20 km) require further investigation (e.g., Álvarez-Valero et al., 2015; Pla and Álvarez-Valero, 2015). The distribution, size, quantity and morphology of bubbles in acidic magmas prior to eruption is under active research (e.g., Wallace et al., 1995; Gualda and Anderson, 2007; Baker et al., 2012). In particular, a better understanding of bubble behavior at depths greater than 2 km is required in order to constrain the influence of magmatic buoyancy and magma chamber overpressure in driving eruptions (e.g., Malfait et al., 2014), as well as the depth at which melt-gas separation starts via bubble nucleation. The occurrence and dynamics of explosive eruptions mainly depend on the initial volatile content of the magma, the ability of gases to escape during its ascent, the viscosity as proxy for diffusivity of volatile species, solubility vs. composition, and pressure. In order to advance in these aspects, we examine El Hoyazo volcano (a Neogene silicic lava dome in SE Spain) with the aim of finding out: (i) when and where bubbles nucleated under the volcano, and (ii) how the porosity varies along the dike as a function of depth. We explored how magmatic bubbles and volatiles evolve during rapid ascent, and their relations to eruptive potential by integrating (i) visual analysis of dacitic samples using SEM and X-ray micro-computed-tomography (micro-CT) (e.g., Gualda and Rivers, 2006; Polacci et al., 2006; Baker et al., 2012); (ii) petrologic depth estimates of the crustal xenoliths and (iii) stable isotope ratios in xenoliths and dacites, to constrain the open vs. closed nature of the system at the depth within the dike where dacite magma and xenoliths came into contact. We then utilized the magmatic porosities and depths to derive a rate of bubble formation during magma ascent towards eruption at El Hoyazo.

1.1. Previous petrological and geochemical results for partially melted crustal xenoliths and their host dacites

The Neogene Volcanic Province (NVP) of SE Spain (Fig. 1) contains high-K calc-alkaline and shoshonitic lava series, which are peraluminous. Lithologically these are largelly calc-alkaline dacites rich in K_2O, with volatile contents from 2 to 4 wt% (mainly H_2O, CO_2) (Zeck, 1970; Benito et al., 1999). These dacites host crustal xenoliths –mainly medium to coarse-grained granulite-facies rocks– with a restitic bulk composition depleted in silica and enriched in aluminium and iron (Zeck, 1970; Cesare et al., 1997; Benito et al., 1999; Duggen et al., 2004). The xenoliths were quenched immediately after eruption (e.g., Zeck, 1970; Cesare et al., 1997; Álvarez-Valero and Waters, 2010), so their microstructures provide a snapshot of the anatectic conditions at depth (e.g., Zeck, 1970; Cesare et al., 1997; Álvarez-Valero and Kriegsman, 2007). El Hoyazo (Fig. 1) was a submarine lava dome with a ~500 m crater radius, and is overlain by Miocene reef carbonates. It is a small circular outcrop of c. 0.7 km^2, which dacites include up to 15% in volume of crustal material (Zeck, 1970). Its atoll geomorphology shows an inner depressed part of mainly dacitic material that corresponds to the old volcanic cone, whereas the top relief is composed by the reef carbonates formed onto the volcanics, which host the crustal xenoliths. Crustal xenoliths and their host dacites are ramdonly collected within the inner part.

The mineralogical and chemical features of the dacite hosting the xenoliths are described, among others, by Zeck (1970) and Benito et al. (1999). The dacite is porphyritic, with >50 vol.% of rhyolitic glassy matrix (both fresh and devitrified), and phenocrysts of mainly plagioclase, biotite, cordierite, and minor orthopyroxene, amphibole, magnetite and ilmenite. Xenocrysts of garnet and quartz are locally present. The xenoliths relevant for this study, i.e. those from the deepest zone detected, are texturally dominated by coarse-grained biotite, elliptical garnet, and large foliated mats of fibrolitic sillimanite, that is locally overprinted by spinel crystals rimmed by melt and minor cordierite. Glass is partially recrystallized to plagioclase, K-feldspar and thin laths of high-Ti biotite. The microtexture of the fibrolitic matrix has a relatively high proportion of glass, and is rimmed by glass against other phases. Spinel porphyroblasts are idioblastic and zoned, both texturally and compositionally (see also Álvarez-Valero and Kriegsman, 2007; Álvarez-Valero and Waters, 2010). The shallowest xenoliths are of the Spl-Crd-M type. The garnet is surrounded by coronas, and the overall parageniesis is Spl-Crd-Pl-Kfs-M.
The coronas mimic the outline of the previous garnet, whose breakdown reaction has been described in detail by Álvarez-Valero et al. (2007). Sillimanite occurs as aggregates of fine needles (fibrolite) in the glass.

Glass mostly occurs as inclusions in garnet and plagioclase, and as microveins of devitrified material, as well as intergrown with fibrolite. Melt inclusions exhibit either rounded or regular, negative-crystal shapes. As outlined by Cesare et al. (1997), their textural position within host phases is compatible with a primary trapping (Roedder 1984). Glass is transparent, showing no evidence for devitrification or crystallization. The bubbles are essentially empty, shrinkage bubbles, with no detectable Raman-active components. Fluid inclusions are rare and restricted to biotite-poor xenoliths. These inclusions contain CO_2-dominated fluids (Cesare et al., 2004).

Direct evidence of partial melting and melt extraction in the xenoliths is provided by the occurrence and high abundance of fresh glass (quenched melt), which occurs as an interstitial phase in layer-parallel films of the matrix and as both devitrified and fresh pockets (Zeck, 1970; Cesare et al., 1997). Glass is also enclosed by all minerals, indicating that all minerals crystallized in the presence of a melt phase, i.e., during partial melting. The presence of intergranular melt films suggest that melt was present during grain growth (by incongruent melting reactions), during subsequent (re)crystallization steps, and after recrystallization of restitic phases had ceased. Melt in inclusions and intergranular films of xenoliths is chemically different from the glass of the dacite host, which has lower Al/Si and higher K/Na ratios (Cesare et al., 1997). Based on mass balance calculations between melt inclusions, xenoliths and potential metapelitic sources, a high degree (35–60 wt %) of melt extraction has been estimated at El Hoyazo (Cesare et al., 1997).

Numerous isotopic studies have demonstrated that mafic magmas that formed in the mantle or lower crust interact with felsic mid-crustal magmas and country rock to produce so-called hybrid magmas (e.g., Benito et al., 1999; Duggen et al., 2004;

Leeman et al., 2008). The NVP dacites are the result of mixing between rhyolites extracted from partially melted pelitic crust and basalts derived from mafic underplating of the Betic Cordillera (e.g., Benito et al., 1999; Duggen et al., 2004; Álvarez-Valero and Kriegsman, 2007).

Microstructures and age relationships in the xenoliths indicate that they first underwent a stage of migmatization and melt extraction, where the rhyolite mixed with the primary basalt to form the host dacites (Duggen et al., 2004; Álvarez-Valero and Kriegsman, 2007). A second sequence of melt-bearing reaction microstructures, developed in a transiently heated wall-rock profile adjacent to the magma conduit, triggered the collapse of the crustal container walls resulting in the brief residence of xenoliths in a dacitic magma at c. 850ºC (Álvarez-Valero and Waters, 2010). The xenoliths experienced rapid transfer from depth to the surface during the eruption, with minutes to hours separating the xenoliths partial melting and their preservation by post-eruptive quenching (Álvarez-Valero and Waters, 2010; Álvarez-Valero et al., 2015; Pla and Álvarez-Valero, 2015).

2. Methods

The provenance depths of the crustal xenoliths below El Hoyazo are well constrained at c. 6 and 4.5 Kbar through thermodynamic modeling (i.e. ~ 19 and 13 km depth, respectively; Table 1; see also Álvarez-Valero and Waters, 2010 for details of the pressure estimates). These depths define a precise section of the volcanic dike. Hence, in order to track the bubbles evolution at depth along the dike, we selected twelve dacites from within few centimetres of a hosted xenolith that quenched simultaneously. In other words, these dacites host a variety of crustal xenoliths, which served as samples of restite from various known depths (Álvarez-

Valero and Waters, 2010) under El Hoyazo volcano (Table 1; Fig. 1). They were analyzed for the stable isotope ratios of hydrogen and oxygen (δD, $\delta^{18}O$). Four of them were selected for X-ray micro-Computed Tomography (micro-CT) and Scanning Electron Microscope (SEM) analysis (samples HY-14-2; HY-14-8; HY-14-9; HY-14-10). Location coordinates are not useful in this studied case as the xenoliths occur randomly distributed within the entire outcrop.

2.1. Stable Isotope Analysis

Oxygen isotope analyses of dacites and xenoliths, as well as single xenocrysts, were done at the Servicio General de Analisis de Isotopos Estables, University of Salamanca, Spain, on whole-rock powders by laser fluorination (Clayton and Mayeda, 1963), employing a Synrad 25 W CO_2 laser (Sharp, 1990) and ClF_3 as reagent (e.g., Borthwick and Harmon, 1982). Isotope ratios were measured on a VG-Isotech SIRA-II dual-inlet mass spectrometer. Both internal and international reference standards (NBS-28, NBS-30) were run to check accuracy and precision. Results are reported in $\delta^{18}O$ notation relative to the Vienna Standard Mean Ocean Water (V-SMOW) standard, using a $\delta^{18}O$ value of 9.6‰ for NBS‑28 (quartz) for the mass spectrometer calibration. Long-term reproducibility for repeated determination of reference samples was better than ±0.2‰ (1σ).

D/H ratios were determined on a second SIRA-II mass spectrometer, on H_2 gas obtained by reduction over hot depleted-U of the water released by induction heating of samples, using a vacuum line (Bigeleisen et al. 1952), following the procedures described by Godfrey (1962), with modifications (Jenkin, 1988). Samples were loaded into degassed platinum crucibles that were placed in quartz reaction tubes and heated under vacuum to 125°C overnight to remove any adsorbed H_2O. The yield of evolved gas was used to determine the amount of structural water contained in the sample. Results are reported in δD notation relative to the V-SMOW standard, using a δD = - 66.7 ‰ for NBS-30 (biotite) for the mass spectrometer calibration. Long-term reproducibility for repeated determination of reference samples was better than ± 2 ‰ (1σ). The fractional extraction and purification of fluids (liquid, gas) from glass inclusions was performed by means of a step-heating device.

2.2. X-ray micro-Computed Tomography (micro-CT) and Scanning Electron Microscope (SEM)

Samples were imaged by using two different microtomographs; a ScanXmate-D180RSS270 (Comscantecno Co., Ltd.) at Tohoku University, and an Argus (SUINSA Medical Systems) at the University of Salamanca (USal), to characterize the 3D morphology, distribution and volume of bubbles within dacites during ascent from c. 19 to 13 km depth. The tomographic scans were performed at 150 kV and 110 μA. The source-to-detector distance was 670.094 mm, while the sample-to-detector distance was 39.747 – 63.403 mm. Each sample was set on a rotation stage, and transmission images were obtained for each 0.18˚ of rotation, to a total of 2000 images. The isotropic pixel edge sizes ranged between 7.53 and 12 μm.

Three-dimensional (3D) analyses were reconstructed from the transmission images by using an original software package called ‘‘Slice’’ (Okumura et al., 2008). A representative volume for each sample was selected in order to avoid exposed surfaces and to remove fractures due to sample preparation (see Table 1).

The SEM images were segmented to separate bubbles from glass and crystals. The segmentation consists in the choice of a threshold, in order to obtain binary images where the vesicles are isolated from the dacite. For the binarization, we translated CT values to 8 bit values and then made binary images using a threshold value in 8 bit images, which allowed us to separate the vesicles from the dacite.

Next crystals in the magma need to be individualized from its glassy matrix. To this end, a pre-segmentation step is usually required to increase the contrast between different phases and to remove background noise, as both crystals and glassy matrix in a sample may have similar X-ray attenuation coefficients (e.g., Zandomeneghi et al., 2010; Voltolini et al., 2011). However, for most of the samples considered (HY-14-10, HY-14-8 and HY-14-2), the contrast between crystals and their embedding matrix was enough as not to require segmentation. Only sample HY-14-9 required application of a bilateral filter (Tomasi and Manduchi, 1998) by using "ImageJ" software (Abramoff et al., 2004), in order to better distinguish the crystals from their glassy matrix, reducing the noise and potential artifacts while preserving edges and the shape of the objects. This type of image processing separated bubbles, glass and crystals, and allowed us to calculate bubble abundances and dacite porosity. We then calculated the bubble number density (BND = number of bubbles / volume of glassy groundmass) and bubble size distribution (BSD) (Cashman and Mangan, 1994; Hurwitz and Navon, 1994; Mangan and Cashman, 1996; Gardner et al., 1999; Larsen and Gardner, 2000; Blower et al., 2001, 2002; Toramaru, 2006; Bai et al., 2008; Polacci et al, 2008, 2009; Baker et al. 2012; LaRue et al., 2013; Masotta et al., 2014) (see Table 1b). BSD and BND can be used to discern between single or multiple nucleation events during the magma ascent (Bai et al., 2008).

In addition, we utilized SEM visual analysis (secondary electron detector) at the Centro de Láseres Pulsados (USal) to check for the presence of bubbles below the detection limit of micro-CT. The SEM used an Extra High Tension of 10.94 kV, Working Distance of 6-17 mm, and Irrigating Probe at 32 pA.

3. Results: Stable Isotopes, micro-CT and SEM

Oxygen and hydrogen isotopic ratios in dacite were $\delta^{18}O$=15.4±0.2‰ and δD=-87.1±3.3‰ (1σ, n=4), respectively. In the xenoliths, whole rock measured values were marginally lighter (although this effect may be attributed to one single sample) and more variable, at $\delta^{18}O$ = 15.3 ± 0.6‰ and δD = - 89.2 ± 9.4‰ (1σ, n=4). When mineral separation could be achieved, oxygen isotopic ratios were always higher in the xenoliths than in the host dacite (see Table 2; Fig. 2). The unusually high values of the oxygen isotopic ratios measured are in line with values reported by Benito et al. (1999) for the NVP in general and El Hoyazo in particular.

3.1. Shallow samples (i.e., at 13 km depth)

Of the samples available, HY-14-10 corresponds to the shallowest levels. Measured values for the dacite were δD = -89.2‰ and $\delta^{18}O$ = 15.1‰, while the crustal xenoliths gave δD = -85.5‰ and $\delta^{18}O$ = 14.5‰ (Table 2). The estimated porosity in the dacites is 6.4% and its BND is 235 mm^{-3} (Table 1; Fig. 3). BSD results indicate a significantly higher number of small size bubbles than those of large size (Fig. 4). SEM images reveal local orientation trends of the bubbles in the dacites (Fig. 3f), as well as irregular geometries (e.g., Fig. 5a, c).

3.2. Deep samples (i.e., at 19 km depth)

Sample HY-14-9 comes from the deepest part of the dacitic dyke (Fig. 3, a,b) δD and $\delta^{18}O$ values are -88.5 and 15.1, respectively. The crustal xenoliths within this sample gave δD = -102.8‰ and $\delta^{18}O$ = 15.7‰ (Table 2). In the dacite, the porosity is 1.7 % and its BND is 763 mm^{-3} (Table 1; Fig. 3). BSD estimates reveal that the number of bubbles of small size is higher than those of larger size (Fig. 4). SEM images indicate that deep dacites often show elongated bubble geometries (e.g., Fig. 5e, g).

Simple first order estimates of bubble growth according to results shown in Fig. 4, i.e., how much does a bubble varies (in terms of size) as pressure drops, when other key parameters are in equilibrium (namely e.g., the amount of gas species degassing into the bubble from the surrounding silicate liquid per unit time, itself dependent on the initial volatile composition of the melt, its viscosity and surface tension, and kinetics) hints at an average bubble size enlargement of up to 13 mm^3/Kbar.

4. Discussion

4.1. Dacite depths: Coeval quenching at the contact with crustal xenoliths

Phase diagram modeling (Álvarez-Valero and Waters, 2010) and numerical simulations (Álvarez-Valero et al., 2015; Pla and Álvarez-Valero, 2015) for El Hoyazo volcano, indicate that the magma ascended from c. 19 to 13 km depth in the range of minutes to hours. Measured isotopic ratios are consistent with this scenario: average $\delta^{18}O$ and δD are indistinguishable from each other in dacites and their xenoliths (Fig. 2, Table 2). Equilibrium / disequilibrium relations established at depth were preserved during rapid ascent and quenching of the magma, that had no time to reset isotopic ratios, and inherited, therefore, $\delta^{18}O$ and δD values acquired at high temperature (i.e., c. 850°C) in the magma source region. If anything, there is hint for heavier δD values and lower water contents in shallower samples (HY-14-10) relative to deep ones (HY-14-9), present in both dacites and their xenoliths.

The δD-H_2O isotope systems allow us to determine whether or not gas is able to decouple from melt via open-system degassing (e.g., Taylor et al., 1983; Newman et al., 1988; Castro et al., 2014). In other words, the isotopic change in a perfectly closed (and theoretical) system exhibits a linear trend by following the mass balance equation of Taylor et al. (1983) where δD decreases moderately for a relatively large decrease in the bulk H_2O in solution in the magma. Comparing the deepest (HY-14-9) with the shallowest (HY-14-10) sample, our results show that δD actually increases from bottom to top, at the time that H_2O contents become similar or slightly lower. If the El Hoyazo system behaved as an open system, different opposite situations would be expected (i.e., either open system water degassing or hydration should result in lower δD; Taylor et al., 1983; Newman et al., 1988). This indicates that the magmatic system below El Hoyazo did not detect significant additions of external volatiles during magma ascent, nor experienced significant fluxes of volatiles from the surrounding crust.

Local microtextures in the dacites are similar to those in the xenoliths, involving similar mineral assemblages, namely biotite-hercynite-cordierite-melt and garnet-biotite-cordierite-melt (Fig. 1c, d, e). This suggests that the dacites were also partly quenched at those particular depths, i.e., 19 and 13 Km (see also Newmann et al., 1988). Xenolith textures were the result of an anatectic episode, that produced large amounts of melt that escaped from the pelitic country rocks (as described by Zeck, 1970), resulting in migmatization (and quenching) (Álvarez-Valero and Waters, 2010). This event was prior and independent of the transient melting event that rapidly erupted the dacites, transporting all xenolith types to the surface. Therefore we inferred the provenance depth of the dacites, and in turn their measured variation of porosity from 1.7 to 6.4 % between 19 and 13 km depth (Table 1), from the pressure at which their hosted metapelitic xenoliths equilibrated. We state that, otherwise, during the ascent from 19 to 13 km, the different magmatic and porosity microtextures may show evidence of magma fragmentation (e.g. Eichelberger, 1995), or been homogenized during their ascent from 13 km depth to the surface. This agrees with recent experimental constraints (e.g., Brugger and Hammer, 2010; Cichy et al., 2011), which demonstrated that changes in mineral assemblage, crystal abundance, variation in mineral compositions and texture are related to isothermal magma ascent and decompression rates.

Therefore given that the exposed dacites are not homogenized in terms of porosity in El Hoyazo, we speculate that rapid magma ascent may also have inhibited bubble and crystal nucleation above 13km (e.g. Mangan and Sisson, 2000; Lloyd et al., 2014). In other words, a rapid ascent above 13 km depth may favour a delay in the nucleation process.

4.2. Correlation between porosity and depth

The volume of bubbles in an erupted volcanic rock may not necessarily reflect the P-T conditions at which the bubbles formed in the dike, since processes such as outgassing and late-stage crystallization may occur during magma ascent. These processes can promote irregular bubble shapes between the microlites (Fig. 5a) due to the collapse of the bubble. This collapse is promoted by the relaxation timescale that depends on the surface tension of the bubble as well as the melt viscosity. It is widely accepted that when a melt supersaturated with volatiles is depressurized, small clusters of gas molecules nucleate and grow through volatile diffusion in the melt (e.g., Toramaru, 1995; Proussevitch and Sahagian 1996, 1998). We focus on vesicle growth at depth (Fig. 3), not on the initial nucleation process, which is beyond the scope of this contribution. The growth of gas bubbles mainly requires volatile diffusion from the melt into pre-existing bubbles, as growth is kinetically favoured over nucleation when the degree of supersaturation is low enough as not to achieve the necessary nucleation pressure. This also depends on the volatile composition of the melt, its viscosity and surface tension (e.g., Mangan and Sisson, 2005; Masotta et al., 2014). Another important driver of bubble growth is the mechanical expansion due to decreasing ambient pressure (e.g., Proussevitch et al. 1993; Sparks et al. 1994; Huber et al. 2014).

The consistency of groundmass and crystal volumes between 19 and 13 km depth supports that little late-stage crystallization occurred (Table 1, Figs. 3 5), whereas the local orientation trends of the bubbles (Fig. 3e) may be related to the stress conditions at the dike's wall, that were not homogenized at the shallow vent depths. Along the 6 km-dike dacites show similar water contents and microtextures, indicating uniform conditions during magma ascent and degassing (Martel et al., 2000). In addition, the relationship between porosity (Table 1) and dissolved water match the quantitative trends in the multicomponent liquid–gas equilibrium in a silicic system of Papale et al. (2006). Outgassing during rapid feeder dike emplacement is nearly constant at low porosity (Takeuchi et al., 2009), likely due to the opening and healing of fractures on short timescales, followed by densification of the dome dacites, along the shallow parts of the conduits (e.g., Okumura et al., 2010).

The presence of crystals (c. 25 % of mainly plagioclase, biotite and hornblende; Figs. 3, 5) may have reduced the activation energy for the nucleation of bubbles, and induced nucleation at 13 km that increased the number of bubbles (confirmed by BND and BSD, Table 1 and Fig. 4). Since crystals are normally present at magma storage conditions in natural magmatic systems, heterogeneous nucleation is often expected (e.g., Mangan et al. 2004), especially in the studied case, where the interstitial melt contains crystals and is not supersaturated (e.g., Hurwitz and Navon 1994). Furthermore, the occurence of bubbles is not systematically related to any particular crystal distribution or type (Fig. 3). Therefore, bubbles growth within the El Hoyazo volcano was related to heterogeneous nucleation.

Our results indicate that (i) the porosity in the dacites increases upward from 1.7 to 6.4% (i.e., from 19 to 13 km depth, respectively), thus yielding a porosity opening rate of 0.78 % /km (see also Table 1), and an average bubble growth of up to 13 mm^3/Kbar (see also Fig. 4); (ii) BND values of 763 and 235 mm^{-3} for the deep and shallow samples, respectively, are in line with both bubble nucleation clustering around grain boundaries (microlite, xenocryst, xenolith) at higher depths (Figs. 3, 4, 5), as well as higher coalescense at 13 km than at 19 km depth. Deep bubble formation contributes to crustal overpressure (e.g., Malfait et al., 2014) and to the lubrication of crystal-rich magmas (e.g., Pistone et al., 2013).

Therefore, the presence of small amount of bubbles between 19 and 13 km allows a better understanding of the rapid magma ascent rates obtained from numerical simulations by Álvarez-Valero et al. (2015) and Pla and Álvarez-Valero (2015). Hence, deep bubble formation must be included in evaluations of silicic magma eruptivity (e.g., Takeuchi, 2004; Gottsmann et al., 2009).

CONCLUDING REMARKS

- Bubble nucleation and volume in the deep magma dike increase during ascent-driven decompression at a lower rate and to a lower extent than has been described for shallow vents.

- Rapidly ascending magma at El Hoyazo volcano experiences negligible late-stage crystallization and bubble nucleation at depths above 13 km below the surface.

- The present porosity rate of 0.78 %/km may be used in silicic subvolcanic systems as an approximation in models and experiments for a better understanding of deep bubble formation, and if necessary, to accurately evaluate magma eruptibility.

- Silicic lava domes hosting crustal xenoliths are extraordinary scenarios to study different bubble snapshots along their evolution during ascent in a deep dike. We provide evidence of how bubbles may behave within the deep silicic dike beneath El Hoyazo. Our results can be used as a proxy for crystallization and bubble formation beneath contemporary volcanoes, and help improving the general knowledge of the vesiculation process at varying depths beneath active volcanoes.

Acknowledgements

This research was supported by the D. Samuel Solórzano Foundation (University of Salamanca - project FS/5-2012) and Programa Propio I (Usal-2014) through A.M.A-V, who also thanks the assistance of the Ramón y Cajal research program (RYC-2011-07584), and the facilities at the Centro de Láseres Pulsados (CLPU – Nucleus – USal). M.D. acknowledges the funded stay at the University of Salamanca in 2014 by the MISTI program (Massachusetts Institute of Technology [MIT] International Science and Technology Initiatives). We also thank two anonymous reviewers for their in-depth and constructive comments and suggestions that notably helped to improve this contribution, as well as the careful editorial handling by Nelson Eby.

References

Abràmoff, M.D., Magalhães, P.J., Ram, S.J., 2004. Image processing with ImageJ. Biophotonics international, 11, 36-42.

Álvarez-Valero, A.M., Kriegsman, L.M., 2007. Crustal thinning and mafic underplating beneath the Neogene Volcanic Province (Betic Cordillera, SE Spain): evidence from crustal xenoliths. Terra Nova 19, 266–271.

Álvarez-Valero, A.M., Waters, D.J., 2010. Partially melted xenoliths as a window into sub-volcanic processes: evidence from the Neogene magmatic event of the Betic Cordillera, SE Spain. Journal of Petrology 51, 973-991.

Álvarez-Valero, A.M., Pla, F., Kriegsman, L.M., Geyer, A., Herrero, H., 2015. Observing silicic magma transport in dikes at depths of 8 - 19 km: evidences from crustal xenoliths and numerical modelling. Journal of Volcanology and Geothermal Research 296, 69-79.

Bai, L., Baker, D.R., Rivers, M., 2008. Experimental study of vesicle growth in Stromboli basalt melts at 1 atm. Earth and Planetary Science Letters 267, 533–547.

Baker, D.R., Mancini, L., Polacci, M., Higgins, M.D., Gualda, G.A.R., Hill, R.J., Rivers, M.J., 2012. An introduction to the application of X-ray microtomography to the three-dimensional study of igneous rocks. Lithos, 148, 262-276.

Baker, D.R., Brun, F., O'Shaughnessy, C., Mancini, L., Fife, J.L., and Rivers, M. (2012b) A four-dimensional X-ray tomographic microscopy study of bubble growth in basaltic foam. Nature Communications, 3, 1135.

Benito, R., López-Ruiz, J., Cebriá, J.M., Hertogen, J., Doblas, M., Oyarzun R., Demaiffe D., 1999. Sr and O isotope constraints on source and crustal contamination in the high-K calc-alkaline and shoshonitic Neogene volcanic rocks of SE Spain. Lithos 46, 773-802.

Bigeleisen, J., Perlman, M.L., Prosser, H.C., 1952. Conversion of hydrogenic materials to hydrogen for isotopic analysis. Anal Chem 24, 1536–1537.

Blower, J.D., Keating, J.P., Mader, H.M., Phillips, J.C., 2001. Inferring volcanic degassing processes from vesicle size distributions. Geophysical Research Letters 28, 347–350.

Blower, J.D., Keating, J.P., Mader, H.M., Phillips, J.C., 2002. The evolution of bubble size distributions in volcanic eruptions. Journal of Volcanology and Geothermal Research 120, 1–23.

Borthwick, J., Harmon, R.S., 1982. A note regarding ClF_3 as an alternative to BrF5 for oxygen isotope analysis. Geochimica et Cosmochimica Acta 46, 1665–1668.

Brugger, C.R., Hammer, J.E., 2010. Crystallization kinetics in continuous decompression experiments: implications for interpreting natural magma ascent processes. Journal of Petrology 51, 1941-1965.

Cashman, K.V., Mangan, M.T., 1994. Physical aspects of magmatic degassing I I. Constraints on vesiculation processes from textural studies of eruptive products, Reviews in Mineralogy, 30, 447–478.

Castro, J.M., Bindeman, I.N., Tuffen, H., Schipper, C.I., 2014. Explosive origin of silicic lava: Textural and δD–H_2O evidence for pyroclastic degassing during rhyolite effusion. Earth and Planetary Science Letters 405, 52-61.

Cesare, B., Salvioli Mariani, E., Venturelli, G., 1997. Crustal anatexis and melt extraction during deformation in the restitic enclaves at El Joyazo (SE Spain). Mineralogical Magazine 67, 15–27.

Clayton, R.N., Mayeda, T.K., 1963. The use of bromine pentafluoride in the extraction of oxygen from oxides and silicates for isotopic analysis. Geochimica et Cosmochimica Acta 27, 43–52.

Costa A., Melnik O., Sparks R.S.J., Voight, B., 2007. Control of magma flow in dykes on cyclic lava dome extrusion. Geophysical Research Letters 34, L02303.

Costa A., Sparks R.S.J., Macedonio G., Melnik O., 2009. Effects of wall-rock elasticity on magma flow in dykes during explosive eruptions. Earth and Planetary Science Letters 288, 455-462.

Duggen, S., Hoernle, K., van den Bogaard, P., Harris, C., 2004. Magmatic evolution of the Alboran Region: the role of subduction in forming the western Mediterranean and causing the Messinian Salinity Crisis. Earth and Planetary Science Letters 218, 91-108.

Eichelberger, J.C., Carrigan, C.R., Westrich, H.R., Price, R.H., 1986. Non-explosive silicic volcanism. Nature 323, 598–602.

Gardner, J.E., Hilton, M., Carroll, M.R., 1999. Experimental constraints on degassing of magma: isothermal bubble growth during continuous decompression from high pressure. Earth and Planetary Science Letters 168:201–218

Godfrey, J.D., 1962. The deuterium content of hydrous minerals from the east-central Sierra Nevada and Yosemite National Park. Geochim Cosmochim Acta 26, 1215–1245.

Gonnermann, H.M., Manga, M., 2007. The Fluid Mechanics Inside a Volcano. Annual Review of Fluid Mechanics 39, 321–56.

Gottsmann, J., Lavallée, Y., Martí, J., Aguirre-Díaz, G., 2009. Magma-tectonic interaction and the eruption of silicic batholiths. Earth and Planetary Science Letters 284, 426–434.

Gualda, G.A.R., Anderson, A.T., 2007. Magnetite scavenging and the buoyancy of bubbles in magmas. Part 1: discovery of a pre-eruptive bubble in Bishop rhyolite. Contributions to Mineralogy and Petrology 153, 733–742.

Gualda, G.A.R., Rivers, M., 2006. Quantitative 3D petrography using X-ray tomography: application to Bishop Tuff pumice clasts. Journal of Volcanology and Geothermal Research 154, 48–62.

Hurwitz, S., Navon, O., 1994. Bubble nucleation in rhyolitic melts: ex- periments at high pressure, temperature, and water content. Earth and Planetary Science Letters 22, 267–280.

Jaupart, C., Allègre, C.J., 1991. Gas content, eruption rate and instabilities of eruption regime in silicic volcanoes. Earth and Planetary Science Letters 102, 413–429.

Jenkin, G.R.T., 1988. Stable isotope studies in Caledonides of SW Connemara, Ireland. PhD thesis, Univ. Glasgow, UK.

Klug, C., Cashman, K.V., 1996. Permeability development in vesiculating magmas: implications for fragmentation. Bulletin of Volcanology 58, 87–100.

LaRue, A., Baker, D. R., Polacci, M., Allard, P., Sodini, N., 2013. Can vesicle size distributions assess eruption intensity during volcanic activity?. Solid Earth, 4, 373.

Larsen, J.F., Gardner, J.E., 2000. Experimental constraints on bubble interactions in rhyolite melts: implications for vesicle size distributions. Earth and Planetary Science Letters 180, 201–214.

Malfait, W.J., Seifert, R., Petitgirard, S., Perrillat, J., Mezouar, M., Ota, T., Nakamura, E., Lerch, P., Sanchez-Valle, C., 2014. Supervolcano eruptions driven by melt buoyancy in large silicic magma chambers. Nature Geoscience 7, 122-125.

Mangan, M.T., Cashman, K.V., 1996. The structure of basaltic scoria and reticulite and inferences for vesiculation, foam formation, and fragmentation in lava fountains. Journal of Volcanology and Geothermal Research, 73, 1–18.

Martel, C., Bourdier, J.L., Pichavant, M., Traineau, H., 2000. Textures, water content and degassing of silicic andesites from recent plinian and dome-forming eruptions at Mount Pele.e volcano (Martinique, Lesser Antilles arc). Journal of Volcanology and Geothermal Research 96, 191-206.

Masotta, M., Ni, H., Keppler, H., 2014. In situ observations of bubble growth in basaltic, andesitic and rhyodacitic melts. Contributions to Mineralogy and Petrology, 167, 1-14.

Newman, S., Epstein, S., Stolper, E., 1988. Water, carbon dioxide, and hydrogen isotopes in glasses from the ca. 1340 A.D. eruption of the Mono Craters, California: constraints on degassing phenomena and initial volatile content. Journal of Volcanology and Geothermal Research 35, 75–96.

Okumura, S., Nakamura, M., Takeuchi, S., Tsuchiyama, A., Nakano, T., Uesugi, K., 2009. Magma deformation may induce non-explosive volcanism via degassing through bubble networks. Earth and Planetary Science Letters 281, 267–274.

Okumura, S., Nakamura, M., Uesugi, K., Nakano, T., Fujioka, T., 2013. Coupled effect of magma degassing and rheology on silicic volcanism. Earth and Planetary Science Letters 362, 163–170.

Okumura, S., Nakamura, M., Tsuchiyama, A., Nakano, T., Uesugi, K., 2008. Evolution of bubble microstructure in sheared rhyolite: formation of a channel-like bubble network. Journal of Geophysical Research 113, B07208.

O'Neill, J.R., 1986. Theoretical and Experimental Aspects of Isotopic Fractionation. In: Stable Isotopes in High Temperature Geological Processes, MSA (J.W. Valley, H.P. Taylor, Jr., and J.R. O'Neil, editors), v. 16, p. 1-40.

Papale, P., Moretti, R., Barbato, D., 2006. The compositional dependence of the saturation surface of H_2O + CO_2 fluids in silicate melts. Chemical Geology 229, 78–95.

Pistone, M., Caricchi, L., Ulmer, P., Reusser, E., Ardia, P., 2013. Rheology of volatile bearing crystal mushes: mobilization vs. viscous death. Chemical Geology 345, 16–39.

Pla, F., Álvarez-Valero, A.M., 2015. Biot number constraints on the sub-volcanic crust-magma thermal regime: an integrating approach of numerical modelling and petrology. In: Caricchi, L., Blundy, J.D. (Eds.), Chemical, Physical and Temporal Evolution of Magmatic Systems. Geological Society, London, Special Publications, 422, 207-216.

Polacci, M., Baker, D. R., Bai, L., Mancini, L., 2008. Large vesicles record pathways of degassing in basaltic magmas. Bulletin of Volcanology, 70, 1023–1029.

Polacci, M., Baker, D. R., Mancini, L., Favretto, S., Hill, R. J., 2009. Vesiculation in magmas from Stromboli and implications for normal Strombolian activity and paroxysmal explosions in basaltic systems. Journal of Geophysical Research, B1, 114.

Polacci, M., Baker, D.R., Mancini, L., Tromba, G., and Zanini, F., 2006, Three-dimensional investigation of volcanic textures by X-ray microtomography and implications for conduit processes. Geophysical Research Letters 33, L13312.

Sharp, Z.D., 1990. A laser-based microanalytical method for in situ determination of oxygen isotope ratios of silicates and oxides. Geochimica et Cosmochimica Acta

54, 1353–1357.

Takeuchi, S., 2004. Precursory dike propagation control of viscous magma eruptions. Geology 32, 1001–1004.

Takeuchi, S., Tomiya, A., Shinohara, H., 2009. Degassing conditions for permeable silicic magmas: implications from decompression experiments with constant rates. Earth and Planetary Science Letters 283, 101–110.

Taylor, B.E., Eichelberger, J.C., Westrich, H.R., 1983. Hydrogen isotopic evidence of rhyolitic magma degassing during shallow intrusion and eruption. Nature 306, 541–545.

Tomasi C., Manduchi, R., 1998. Bilateral Filtering for Gray and Color Images: Sixth International Conference on Computer Vision, Bombay, India, 839-846.

Toramaru, A., 2006. BND (bubble number density) decompression rate meter for explosive volcanic eruptions. Journal of Volcanology and Geothermal Research, 154(3), 303-316.

Valentine, G.A., 2012. Shallow plumbing systems for small-volume basaltic volcanoes, 2: Evidence from crustal xenoliths at scoria cones and maars. Journal of Volcanology and Geothermal Research 223–224, 47-63.

Voltolini, M., Zandomeneghi, D., Mancini, L., Polacci, M., 2011. Texture analysis of volcanic rock samples: Quantitative study of crystals and vesicles shape preferred orientation from X-ray microtomography data. Journal of Volcanology and Geothermal Research 202, 83-95.

Wallace, P.J., Anderson, A.T.Jr., Davis, A.M., 1995. Quantification of preeruptive exsolved gas contents in silicic magmas. Nature 377: 612-616.

Woods, A.W., Koyaguchi, T., 1994. Transitions between explosive and effusive eruptions of silicic magmas. Nature 370, 641–644.

Zandomeneghi, D., Voltolini, M., Mancini, L., Brun, F., Dreossi, D., Polacci, M., 2010. Quantitative analysis of X-ray microtomography images of geomaterials: Application to volcanic rocks. Geosphere 6, 793-804.

Zeck, H.P., 1970. An erupted migmatite from Cerro de Hoyazo, SE Spain. Contributions to Mineralogy and Petrology 26, 225–246.

Figure Captions

Figure 1. (a) Location of El Hoyazo volcano within the NVP and map of the Betic Cordillera and Rif; **(b)** Field aspect of a spinel-cordierite-melt (Spl-Crd-M) xenolith type in the dacitic lava of this volcano. Plane-polarized light microscopy views of: **(c)** a xenolith at c. 19 km depth, in contact with its host dacite, which show local textures of mineral equilibria (e.g. biotite-hercynite-melt) that are also found in the xenolith; **(d)** a dacite that show the same chemical reactions and textures as in (c) far from the contact with the xenolith; **(e)** a xenolith at c. 13 km depth, in contact with its host dacite, which show a typical texture in the xenoliths such as garnet xenocryst with a cordierite-plagioclase-melt corona. Microstructures in the xenoliths reveal a first stage of migmatization overprinted by a sequence of melt-bearing reaction microstructures (see the text for details). The microstructural features in the dacites enhance the possibility of partial quenching at depth.

Figure 2. Stable isotopes analysis of El Hoyazo dacitic magma and crustal xenoliths. Dacites and their included xenoliths show negligible $\delta\ ^{18}O$ fractionation between them, which is typical for rapid subvolcanic decompression occurring at high

temperatures (e.g., O'Neill, 1986). The δ D values differentiate the water provenances of dacites and crustal xenoliths.

Figure 3. (a) Scheme (not to scale) of the subvolcanic system at El Hoyazo volcano. Three-dimensional view of samples HY-14-9 **(b)** and HY-14-10 **(c)**, which were in contact with xenoliths equilibrated at c. 19 and 13 km depth, respectively. Glass and minerals were suppressed for clarity. Bubbles are shaded dark grey (the clearer grey, the higher bubbles concentration). **(d)** 2D example view of a single microtomographic slice to highlight –in white (**e**)– the crystals amount vs. groundmass vs. bubbles. Grt: garnet xenocryst; Pl: plagiclase; Hb: hornblende; Bt: biotite. (**f)** view of a single tomographic slice of sample HY-14-10 to highlight the bubbles orientation within the dacite.

Figure 4. Bubble sizes distribution (BSD) diagram in the dacites HY-14-9 and HY-14-10 (see also Figs. 3, 5 and Table 1). BSD shows that at higher depth the number of small size bubbles is higher than at lower depth. In the same way, BSD also reveals that at shallower depth the number of bubbles is lower but of larger size than at higher depth.

Figure 5. SEM-SEI images of the same dacites of Figure 3 revealing the existence of tiny bubbles and fractures that are below the detection limit of the micro-CT, as well as the high groundmass/microlites ratio that indicates a minor influence of a potential late-stage vesiculation process (see Fig. 3). Bubbles in lava HY-14-10 (shallowest one) show more irregular shapes and larger sizes (e.g., **a, c**) than in lava HY-14-9 (deepest dacite) with smaller bubbles and more elongated geometries (e.g., **e, g**). **(h)** Current bubble after an exsolved fluid inclusion in a biotite crystal. The groundmass and crystals volumes are fairly constant along the vertical studied 6 km section of the

dike. The bubbles sizes below the detection limit of the micro-CT indicate that our measurements of the total volumes are minimum.

Table 1. (a) Representative volumes used for porosities estimation of the dacites along c. 19 and 13 km depth within the dike. **(b)** Microtextural parameters utilized for quantitative analysis of BND and BSD calculations. The bubbles sizes below the detection limit of the micro-CT (Fig. 5) indicate that our measurements of the total volumes are minimum. (*) Álvarez-Valero and Waters, 2010; (**) Álvarez-Valero and Kriegsman, 2007.

Table 2. Values of the stable isotopes analysis ($\delta^{18}O$, δD) of El Hoyazo dacitic magma and crustal xenoliths.

Figure1
Click here to download high resolution image

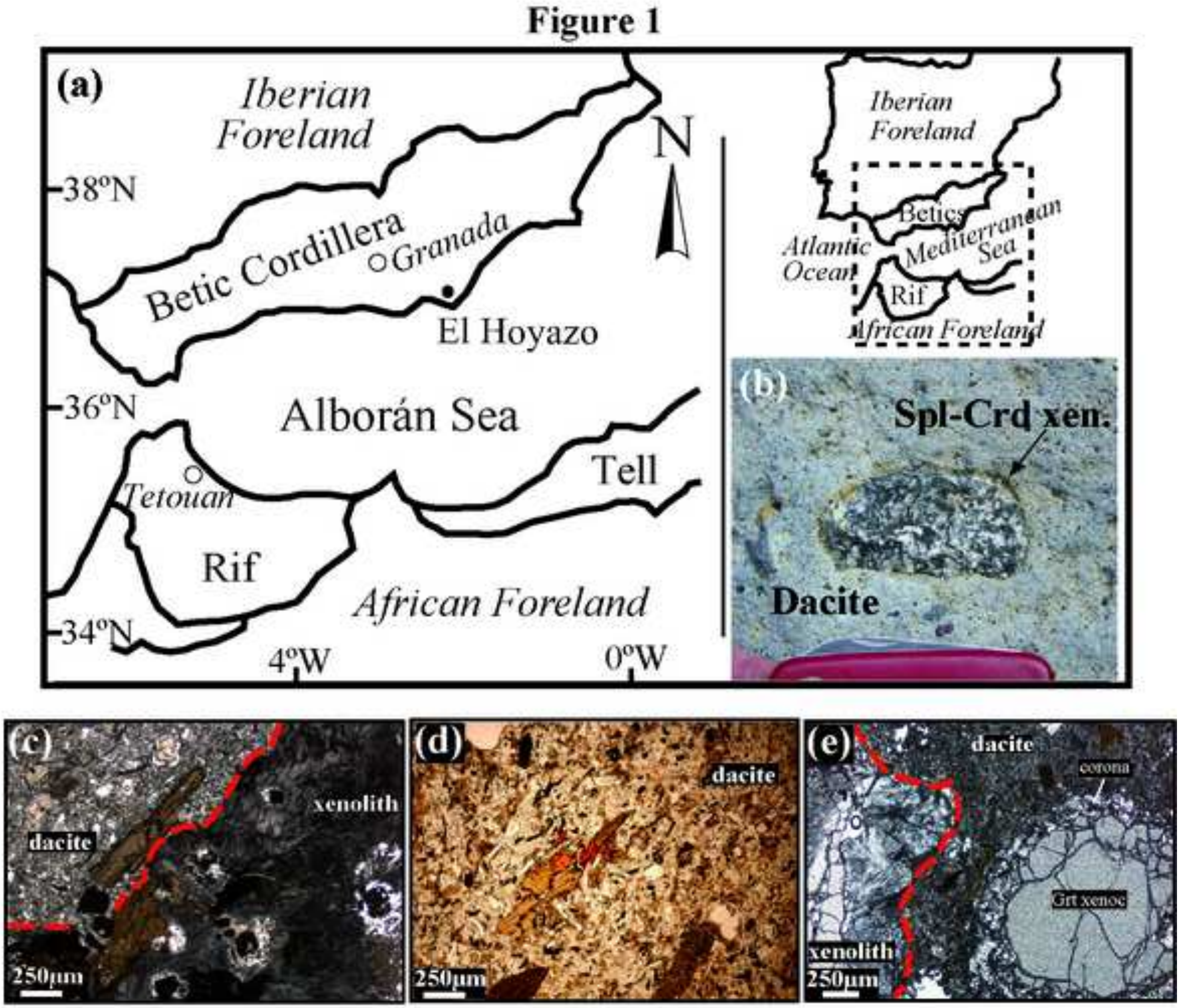

Figure2

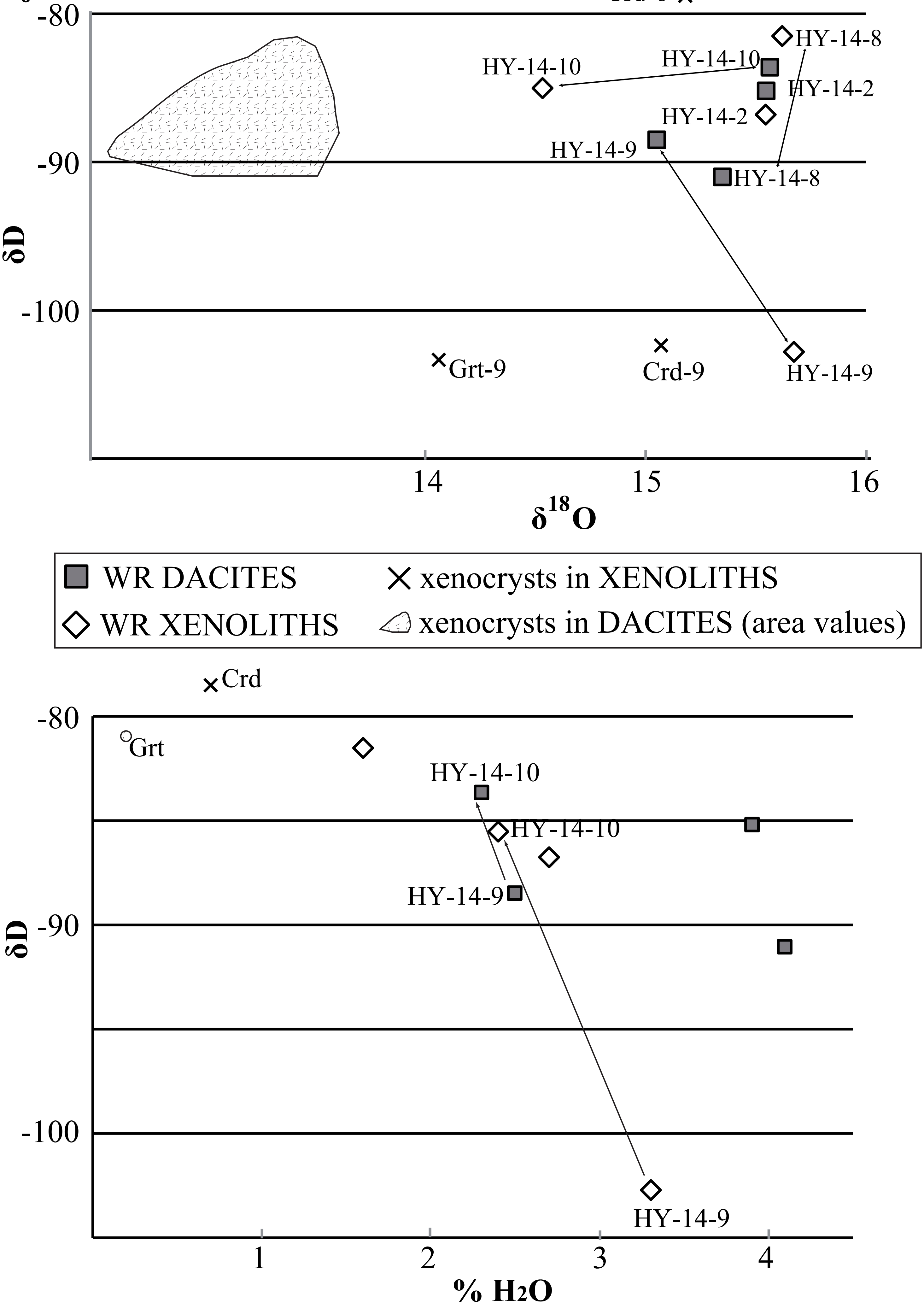

Crd-8
-80
-90
-100
HY-14-8
HY-14-10
HY-14-10
HY-14-2
HY-14-2
HY-14-9
HY-14-8
δD
Grt-9
Crd-9
HY-14-9
14
15
16
δ18O
WR DACITES
xenocrysts in XENOLITHS
WR XENOLITHS
xenocrysts in DACITES (area values)
Crd
-80
Grt
HY-14-10
HY-14-10
HY-14-9
-90
δD
-100
HY-14-9
1
2
3
4
% H2O

Figure3

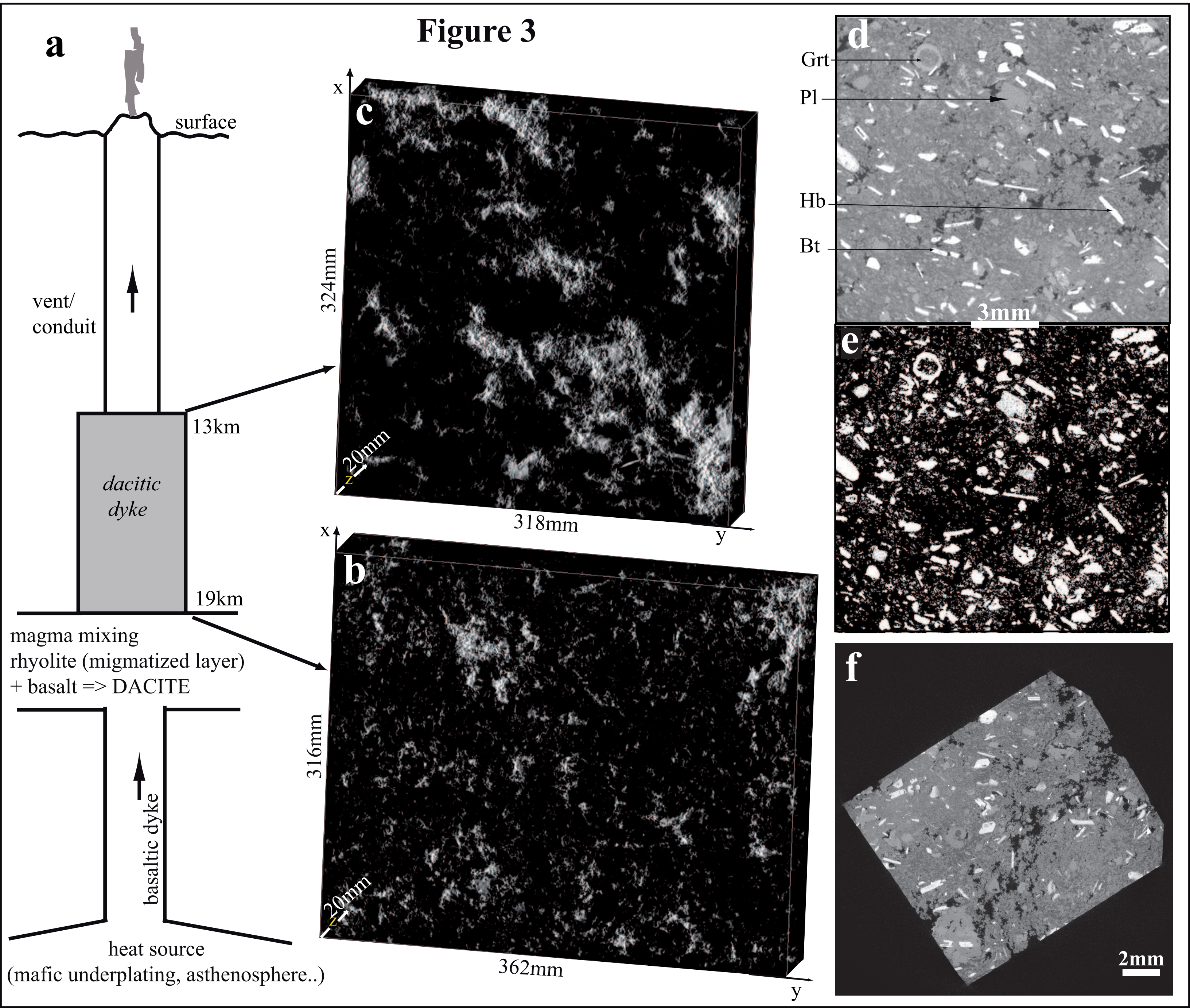

Figure 3
a
surface
vent/
conduit
13km
dacitic
dyke
19km
magma mixing
rhyolite (migmatized layer)
+ basalt => DACITE
basaltic dyke
heat source
(mafic underplating, asthenosphere..)
c
x
324mm
20mm
z
318mm
y
b
x
316mm
20mm
z
362mm
y
d
Grt
Pl
Hb
Bt
3mm
e
f
2mm

Figure4

Click here to download high resolution image

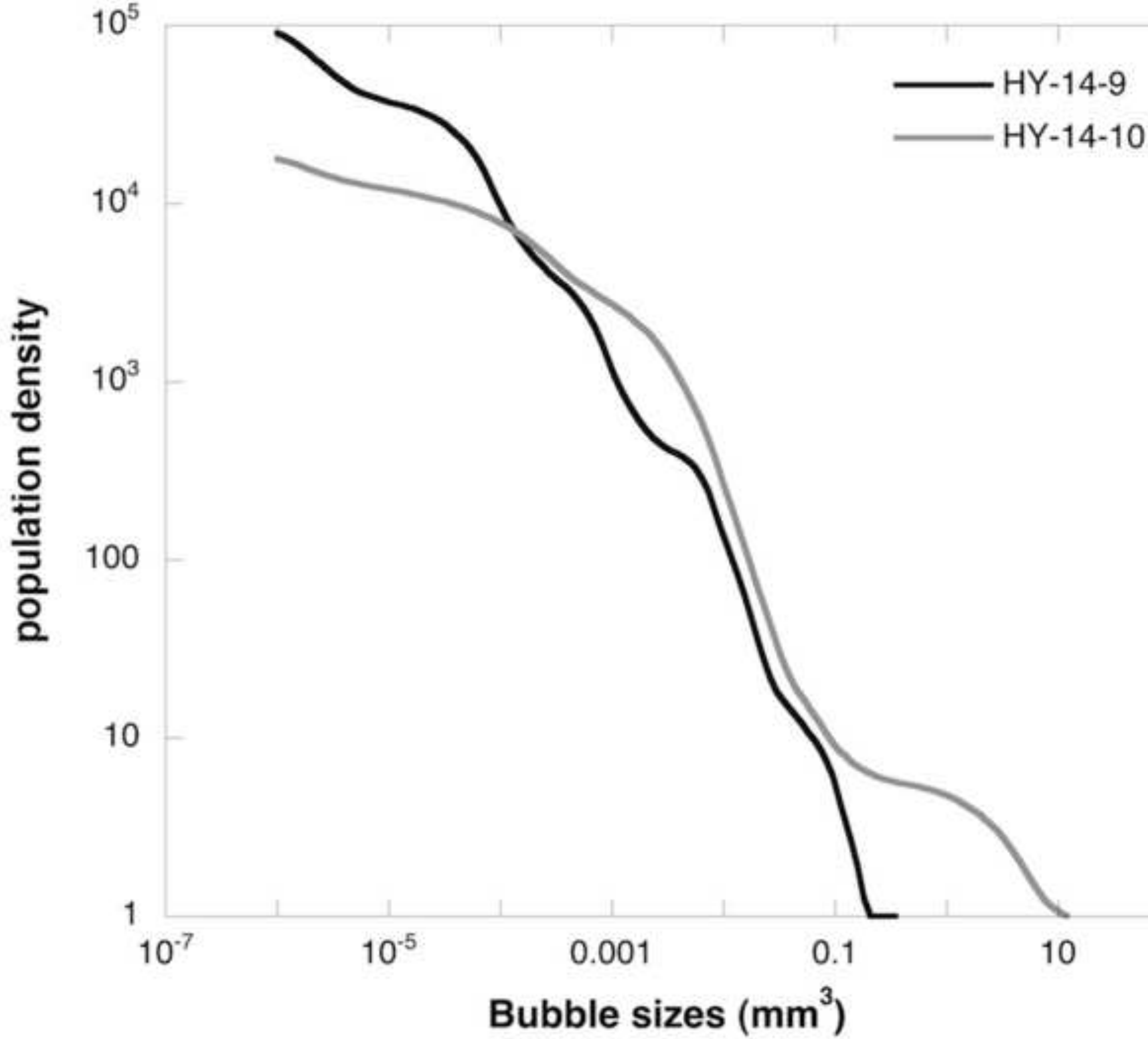

Figure5

Click here to download high resolution image

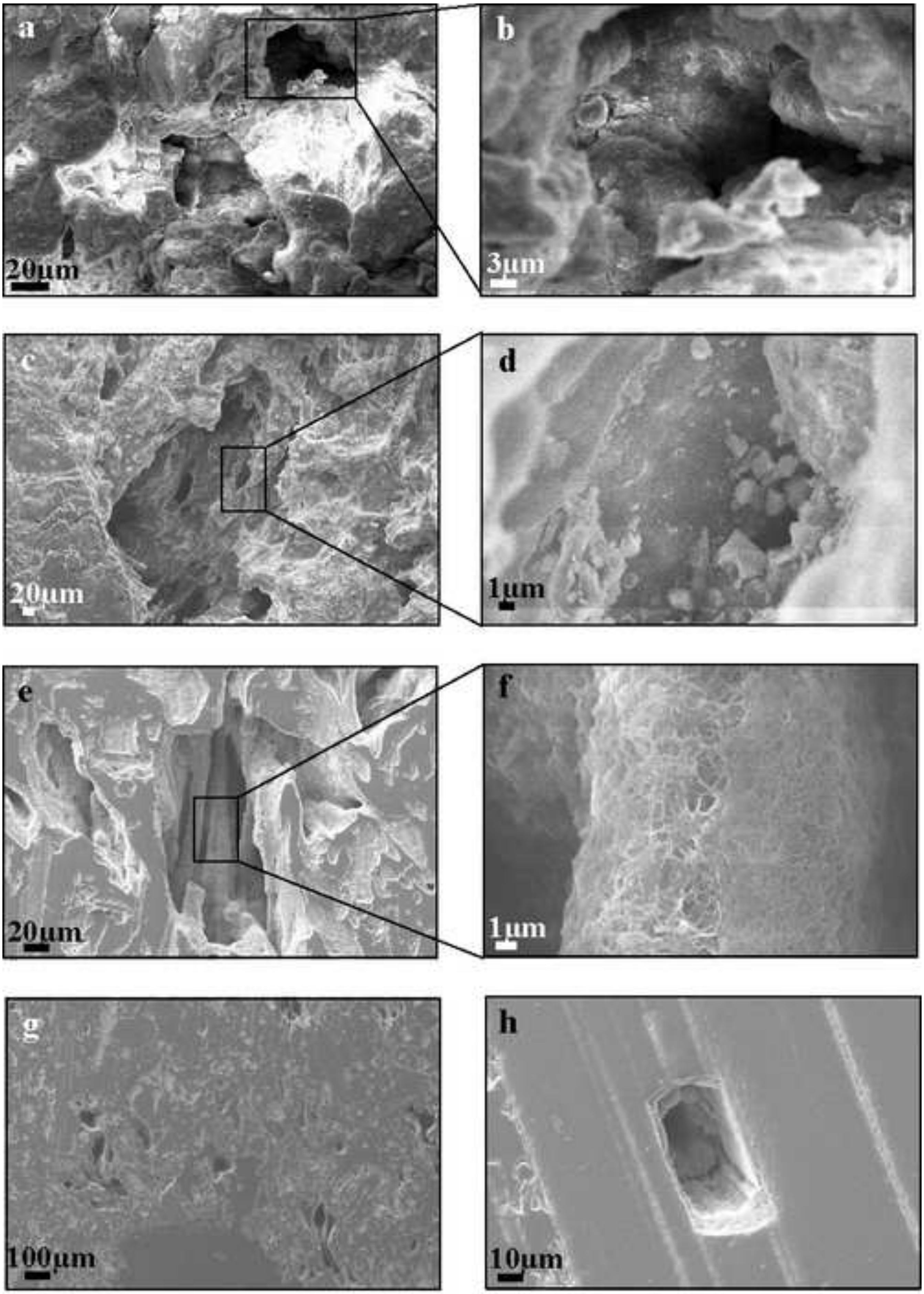

Table1

Click here to download Table: Table 1.xlsx

TABLE 1

Lava Sample	Isotropic pixel edge sizes - (μm)	Total imaged volume (mm3)	Total measured volume (mm3)	BUBBLES Porosity (%)	BUBBLES Volume (mm3)	% H2O (± 0.1) calculated (dacite)	% H2O bulk dacite (estimated from XRF)	Xenolith peak P (kbar, 2σ) metamorphism
HY-14-10	9.96	746	746	6.4	35.0	2.3	3.7 - 4	4.7 ± 0.3 (c. 13 km depth) *
HY-14-8	12.00	966	966	3.1	31.7	up to 4.1		5.7 ± 0.3 (5.4 ~ c. 16.2 km depth) *
HY-14-2	12.00	1084	1084	1.7	18.2			5.7 ± 0.3 (6.0 ~ c. 18 km depth) *
HY-14-9	7.53	322	322	1.7	4.76			6.2 ± 0.8 (c. 19 km depth) **

Sample	Analized volume (pixel)	Analized volume (mm3)	Nº Bubbles	GROUNDMASS Volume (mm3)	CRYSTALS Volume (mm3)	CRYSTALLINITY (%)	BND (mm-3)
HY-14-10	792x522x701	286	43687	185.68	74.1	28.5	235
HY-14-9	870x1100x700	286	159924	209.64	71.6	25.4	763

Table2

Click here to download Table: Table2.docx

Sample	**Type**	**δ^{18}O** (± 0.15)	**δD** (± 1)
HY-14-10	dacite (bulk)	15.6	-83.6
HY-14-8	dacite (bulk)	15.3	-91.0
HY-14-2	dacite (bulk)	15.5	-85.2
HY-14-9	dacite (bulk)	15.1	-88.5
HY-14-10	xenolith (bulk)	14.5	-85.5
HY-14-8	xenolith (bulk)	15.6	-81.5
HY-14-2	xenolith (bulk)	15.5	-86.8
HY-14-9	xenolith (bulk)	15.7	-102.8
HY-14-8	cordierite in xenolith	15.5	-78.2
HY-14-9	cordierite in xenolith	15.1	-
HY-14-9	garnet in xenolith	14.0	-
HY-14-9	plagioclase in xenolith	15.1	-
HY-14-7	garnet in dacite	13.5	-80.9
HY-14-8	garnet in dacite	13.6	-
HY-14-9	garnet in dacite	13.7	-
HY-14-9	quartz in dacite	12.5	-